

Chapter 2

Nanocomposite Based on $\text{Li}_4\text{Ti}_5\text{O}_{12}$ Structures for High-Rate Li-Ion Battery Applications

Ashhan Erdaş, Şeyma Özcan, Deniz Nalci, Mehmet Oğuz Güler,
and Hatem Akbulut

Abstract Lithium titanate is synthesized from titanium isopropoxide and lithium nitrate solution via sol–gel processes. The obtained nanocrystalline lithium titanates were then subjected to electroless deposition in order to obtain $\text{Cu}/\text{Li}_4\text{Ti}_5\text{O}_{12}$ nanocomposite structures. The crystalline structure and morphological observation of the as-synthesized $\text{Li}_4\text{Ti}_5\text{O}_{12}$ are characterized by X-ray diffraction (XRD) and scanning electron microscopy, respectively. It is demonstrated that the electrochemical performance is significantly improved by the copper deposition onto lithium titanate structure. The copper-coated lithium titanate exhibits a stable capacity of 170 mAh g^{-1} at 1 C. Besides, the reversible capacity at 80 C remains over half of that at 1 C. The superior C-rate performance is associated with the copper/lithium titanate nanocomposite structure, facilitating lithium transportation ability during cycling.

Keywords $\text{Li}_4\text{Ti}_5\text{O}_{12}$ • $\text{Cu}/\text{Li}_4\text{Ti}_5\text{O}_{12}$ • Sol–gel • Electroless coating

2.1 Introduction

Lithium-ion (Li-ion) batteries are the now dominating chemistry within battery applications, having 60 % of worldwide sale values in portable batteries [1]. Li-ion chemistries have the highest energy density among the commercialized rechargeable batteries today which originate from their high working potential combined with their high capacities and low weight [1–3]. Yet their performances are not enough for some future demands, which include electric vehicles, power grid load leveling, and peak shaving, which together set a new list of demands on batteries in terms of lifetime, power, and energy density. Inspired by sustainable mobility, Li-ion battery research has focused toward improving the energy and power

A. Erdaş (✉) • Ş. Özcan • D. Nalci • M.O. Güler • H. Akbulut
Department of Metallurgical and Materials Engineering, Faculty of Engineering,
Sakarya University, TR-54187 Serdivan, Sakarya, Turkey
e-mail: aslihan_erdas@hotmail.com

density, under the conditions of safety, long cycle life, and the use of low-cost materials. Therefore, spinel lithium titanate $\text{Li}_4\text{Ti}_5\text{O}_{12}$ (LTO), which is called zero-strain insertion material, has aroused researcher's attention recently, due to its potential application as anode material in high-rate lithium batteries. Spinel host has excellent structure stability and a very small volume change during cycling.

In a typical spinel LTO crystal structure, the 32e positions are occupied by oxygen atoms, while 5/6 of the 16d positions are occupied by Ti atoms, and the rest of the 16d positions are occupied by Li atoms, forming a highly stable $[\text{Li}_{1/3}\text{Ti}_{5/3}]_{16d}\text{O}_4$ framework. The tetrahedral (8a) sites are occupied by Li atoms, while the octahedral (16c) sites are empty, and the structure is denoted as $[\text{Li}]_{8a}[\text{Li}_{1/3}\text{Ti}_{5/3}]_{16d}\text{O}_4$. It is well known that the electronic structure of LTO spinels can be characterized by the empty Ti 3d states with band gap energy of 2–3 eV gives an insulating character to this material which is also reported by Yi et al. [4]. The calculated electrical conductivity of these materials is only $10^{-13} \text{ S cm}^{-1}$ at room temperature. Therefore, low-rate capability due to the low electronic conductivity limits the practical applications, although the electrochemical stability of these electrodes is far beyond the graphite-based commercial electrodes.

Several methods have been proposed to improve these obstacles. Several researches are being carried out to develop the lattice structure of LTOs via reducing the particle size which can shorten the Li-ion diffusion path and provide extended contact area between the electrode and electrolyte, consequently improving Li-ion intercalation kinetics studied by Ladislav et al. [5], Borghols et al. [6], and Naiqing et al. [7]. Another effective way is also reported as the cation doping by incorporating cations of conventional, transition, and rare earth metals by Pierre et al. [8], Kiyoshi et al. [9], Biao et al. [10], and by Damien et al. [11] and anions of F by Shahua et al. [12] and Br by Yanling et al. [13] into the framework of LTO. Surface modifications with high-conductive phases, such as conductive oxides, metals, or carbon-based materials, were also reported by Shahua et al. [14], Yan et al. [15], Arumugam et al. [16], Cheng et al. [17], Zhimin et al. [18], Yonggang et al. [19], Hun et al. [20], Liang et al. [21] and Ilias et al. [22]. It has been previously reported that the surface modification with Ag significantly improved the electronic conductivity of the LTO and which in turn greatly improved the high-rate performance of the LTO by Zhimin et al. [18] and Michals et al. [23]. However, the cost of silver limited the practical applications of LTO-based composites in commercial batteries. On the other hand, copper can be a good candidate due to its low resistivity and high resistance to electron migration and being a cheap and convenient conductive agent when compared with Ag.

From the studies of Yi-R et al. [24, 25] and by Ting et al. [26], LTO synthesis is mostly based on solid-state synthesis using TiO_2 and Li_2CO_3 or LiOH . However, the obtained LTO particle morphologies are mostly in large particle size from submicron to micron range, and these particles contain impurity phases. Therefore, recent reports on LTO synthesis by Wei et al. [27], Meng et al. [28, 29], Zhenjiang et al. [30], Feixiang et al. [31], Daisuke et al. [32], Chien-Te et al. [33], Zhaoyin

et al. [34], Jin et al. [35], and Milica et al. [36] clearly indicate that low-temperature sol–gel, spray drying, and hydrothermal methods are the most efficient procedures for high-purity nanocrystalline LTO structures. In this study, we aimed to produce spinel LTO anode materials with high electronic conductivity. LTO spinel structure is produced via facile sol–gel method, and the surfaces of the spinel LTO particles were then coated with Cu via electroless coating techniques. The effect of copper coating on the electrochemical properties is investigated.

2.2 Experimental Details

2.2.1 Synthesis of LTO Anode Electrodes

LTO powders were produced via sol–gel method using citric acid (Merck, purity: >99 %) as a chelating agent. 5 mmol of titanium isopropoxide, $\text{Ti}[\text{OCH}(\text{CH}_3)_2]_4$ (Sigma Aldrich, %99.999 trace metal basis), was dissolved in 150 mL of 2-propanol (Merck, Emsure) to obtain a saturated solution. 4 mmol of lithium nitrate, LiNO_3 (Merck, purity: 99.995 % Suprapur), was then added with mild stirring. A saturated aqueous citric acid ($\text{C}_6\text{H}_8\text{O}_7$, Merck, >99 %) dissolved in 150 mL of 2-propanol (Merck, Emsure) was then added at a molar ratio of 9 mmol. The pH of the final solution was kept at 7.0 by adding ammonium hydroxide (Alfa Aesar, %25 solution). The solution was then heated to 90 °C with vigorous stirring to remove the excess ammonia and water until a transparent gel was obtained. The gel was then kept for 12 h in air oven at 120 °C in order to obtain metal citrate precipitation. After the drying process, the precursors were decomposed at 450 °C for 4 h and 850 °C for 1 h in air in order to eliminate organic contents.

2.2.2 Electroless Cu Coating of LTO Anode Electrodes

Pristine LTO particles were used as the cores of the composite powders in the electroless plating. Before starting the deposition process, the surfaces of the anode active powders should have to be pretreated as follows: (1) the surfaces of the as-synthesized powders were cleaned by immersing powders into 1 M sodium hydroxide (Merck, Titripur) solution for 10 min. (2) As-cleaned LTO powders were then immersed into boiling hydrochloric acid (Merck, 1 N) for 15 min to coarsen their surfaces. The coarsened surfaces will also help to improve the adhesion between the LTO-based powders and copper particles. (3) Since the surfaces of LTO powders were nonconductive, an activation process is needed in order to improve the catalytic properties. One-step

sensitization and activation process was performed in this study. The etched particles of LTO were immersed in a palladium activation solution consisting of palladium dichloride (Merck, PdCl_2) (0.3 g/L), stannous chloride (Merck, $\text{SnCl}_2 \cdot 2\text{H}_2\text{O}$, >99.9 %) (16 g/L), sodium chloride (Merck, NaCl , >99.99 %) (150 g/l), and hydrochloric acid HCl (Merck, 1 N) (60 mL/L) and stirred strongly at room temperature for 15–20 min. After each pretreatment process, particles of LTO were repeatedly washed by using bidistilled water until pH is reached to 7. The pretreated powders were then dried after the activation step in an oven at 80 °C for 12 h.

2.2.3 Characterization

The crystal structures of the LTO and Cu/LTO anode materials were examined using an XRD spectrometer (XRD, Rigaku D/max 2200) with monochromated $\text{Cu K}\alpha$ radiation at a scanning rate of 1° min^{-1} in the range of 10° – 80° . Surface morphology was examined using SEM (Jeol 6060 LV).

2.2.4 Electrochemical Characterization

Galvanostatic charging and discharging tests were performed using CR2016 coin-type cells by using MTI BST8A battery tester system. The anode electrode was prepared by blending active material, carbon black (Alfa Aesar, >99.9 %), and polyvinylidene fluoride (Alfa Aesar, >99.9 %) (80:10:10) in *N*-methyl-2-pyrrolidone (Alfa Aesar, >99 %) with a weight ratio of 8:1:1. The slurry was casted onto an aluminum foil by the “doctor blade” technique. The weight of active material was $\sim 1.786 \text{ mg cm}^{-2}$. Coin-type (CR2016) test cells were assembled in an argon-filled glove box (Mbraun, Labstar) using a microporous polypropylene film (Celgard 2400) as a separator, 1 M LiPF_6 (Sigma Aldrich, ≥ 99.99 %) in ethylene carbonate (Sigma Aldrich, 99 %) and dimethyl carbonate (Sigma Aldrich, ≥ 99 %) (EC/DMC, 1:1 vol) as electrolyte, and Li foil as the counter and reference electrodes. Constant current charge/discharge was performed at various rates within a voltage window of 1–2.5 V (versus Li^+/Li). Electrical impedance spectroscopy (EIS) experiments were carried out on a Gamry Reference 3000 advanced electrochemical system in the frequency range mainly from 1 MHz to 50 MHz at an amplitude of 10 mV. Before all electrochemical measurements, all samples were aged for 24 h at room temperature.

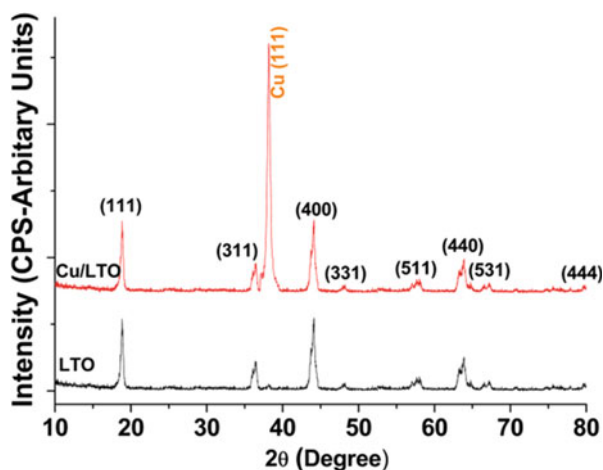
2.3 Results and Discussions

2.3.1 Structural and Morphological Observations

The X-ray diffraction patterns of the synthesized powders are shown in Fig. 2.1. All the sharp diffraction peaks can be indexed on the basis of a cubic spinel structure, $\text{Li}_4\text{Ti}_5\text{O}_{12}$ (JCPDS file no. 26-1198). The peaks at $2\theta = 18.4^\circ$, 35.6° , 43.3° , 47.4° , 57.2° , 62.8° , 66.1° , 74.3° , and 79.3° , which correspond to (111), (311), (400), (331), (511), (440), (531), (533), and (444) planes of a face-centered cubic spinel LTO with a $Fd\bar{3}m$ space group, respectively. This suggests that high-purity LTO can be prepared by calcinating the sol-gel-derived precursors at 850°C for only 1 h. No trace amount of impurity of Li phase can be detected, as shown in Fig. 2.1. In preliminary studies, we found that TiO_2 and Li_2TiO_3 phases would coexist with the main LTO phase when the sintering temperature was lower than 600°C . It is also well known that when increasing the heat treatment temperature, TiO_2 or Li_2TiO_3 would disappear depending on the starting composition, Li rich or Ti rich. The sol-gel synthesis leads to samples with notably higher purity. Indeed, no Li impurities were detected in the X-ray diffraction pattern. The lattice parameters were calculated by the least-squares method using ten diffraction lines, and silicon was used as a reference to calibrate the peak position and intensity ratio. The crystal lattice parameter, a , was also calculated and was 8.359 \AA for the samples, in good agreement with that obtained by Zhu et al. [3]. The crystal size of the LTO crystallites was evaluated by the Scherrer formula and found to be ca. 59 nm using the (111) reflection.

In order to determine the effects of copper coating on the crystal structure of LTO, the X-ray powder diffraction was carried out for uncoated and coated spinel materials and presented in Fig. 2.1b according to the JCPDS 04-0836. The intensities of the LTO peaks were reduced after coating the surfaces of the based spinels

Fig. 2.1 XRD patterns of the (a) pristine LTO and (b) Cu-coated LTO spinel samples



uniformly with copper, which is the expected result. The lattice parameters were also calculated by the least-squares method for copper-coated LTO spinel samples and found to be 8.354 Å. The calculated lattice parameters show that there was almost no change in the lattice parameter for all samples which indicated that copper ions were not incorporated into the spinel structure but are just presented on the surfaces of LTO spinel samples. Hui et al. [37] reported that copper ion introduction to the spinel structure will lead to a significant change of the lattice parameter. The data obtained from the Fig. 2.1b also indicate that copper crystals largely grow in two preferential orientation (111) plane. Hui et al. [37] also reported that the peaks due to copper crystallites with (111) orientation are predominant. This is an important result knowing that stress-induced voiding is significantly inhibited in (111)-textured metals which is also reported by Zhaoyin et al. [34]. Furthermore, the (111)-textured Cu film has higher resistance to electromigration which suppresses grain boundary and interfacial diffusion of metal atoms previously reported by Jin et al. [35].

Surface morphologies of the LTO and Cu/LTO powders calcined at 850 °C are presented in Fig. 2.2. A typical SEM image in Fig. 2.2a shows that the sample has polyhedron morphology and a uniform particle size distribution. Higher magnification SEM image in the inset of Fig. 2.2a indicates that the polyhedron structures are composed of subgrains that have a particle size ranges from 60 to 90 nm, which is in agreement with the XRD result. Figure 2.2b shows the SEM images of

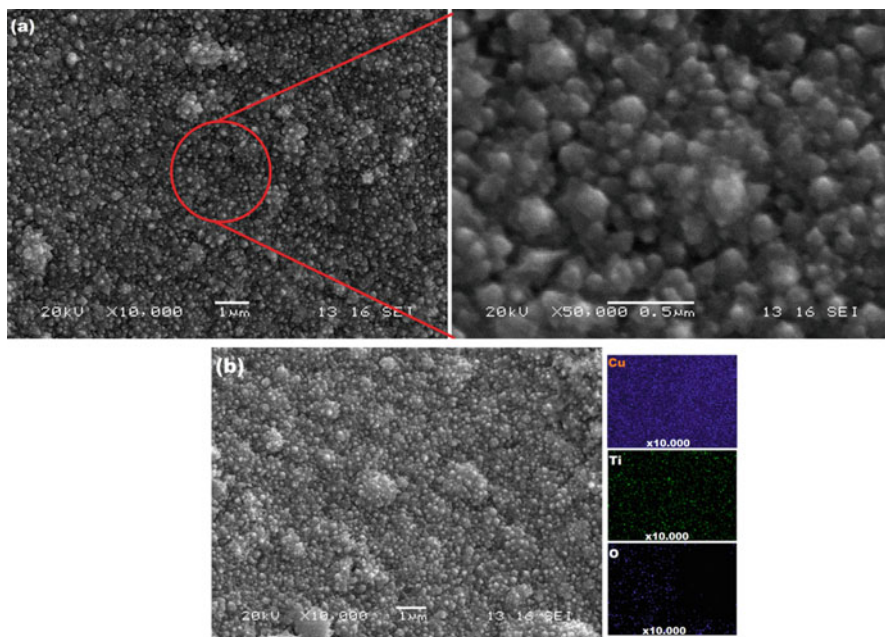


Fig. 2.2 SEM images of the (a) pristine LTO and (b) Cu-coated LTO with EDS Dot map analysis of spinel samples

Cu-coated as-synthesized LTO powders with EDS dot map analysis. No free copper particles and uncoated surface of pristine LTO particles are found in powders. From Fig 2.1a, b, it can also be concluded that surfaces of polyhedrons have not been changed after electroless deposition process from the SEM images. In addition, EDS dot map analysis also confirms that the surfaces of the LTO powders were coated uniformly with Cu.

2.3.2 Electrochemical Results

As shown in Fig. 2.3, only one pair of anodic/cathodic peak is observed in the CV curves of pristine LTO calcined at 850°C . In the first cycle, the cathodic and anodic peaks are at 1.47 and 1.69 V, respectively. These peaks can be regarded as the signature of lithium insertion into and extraction from the spinel LTO framework, which is consistent with the previous studies by Daisuke et al. [32], Chien-Te et al. [33], Zhoyin et al. [34], and Jin et al. [35]. Upon completion of the 1st and 4th cycles, the CV curves still coincide well with that of the first cycles. The well-defined small potential interval between cathodic and anodic peaks and the good overlap of CV curves clearly indicate that the sample has high electrochemical reaction activity and reversibility.

Galvanostatic charge/discharge curves of pristine LTO and Cu/LTO as anode electrodes for Li-ion batteries are evaluated and given in Fig. 2.4. The electrode density and percentage of the active mass were adjusted to be similar for all samples

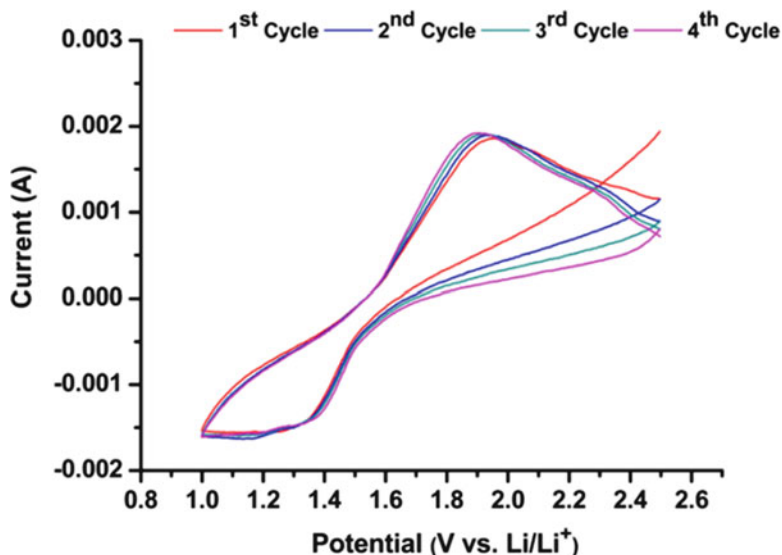


Fig. 2.3 Cycling voltammetry curves of the pristine LTO anode electrodes for four cycles

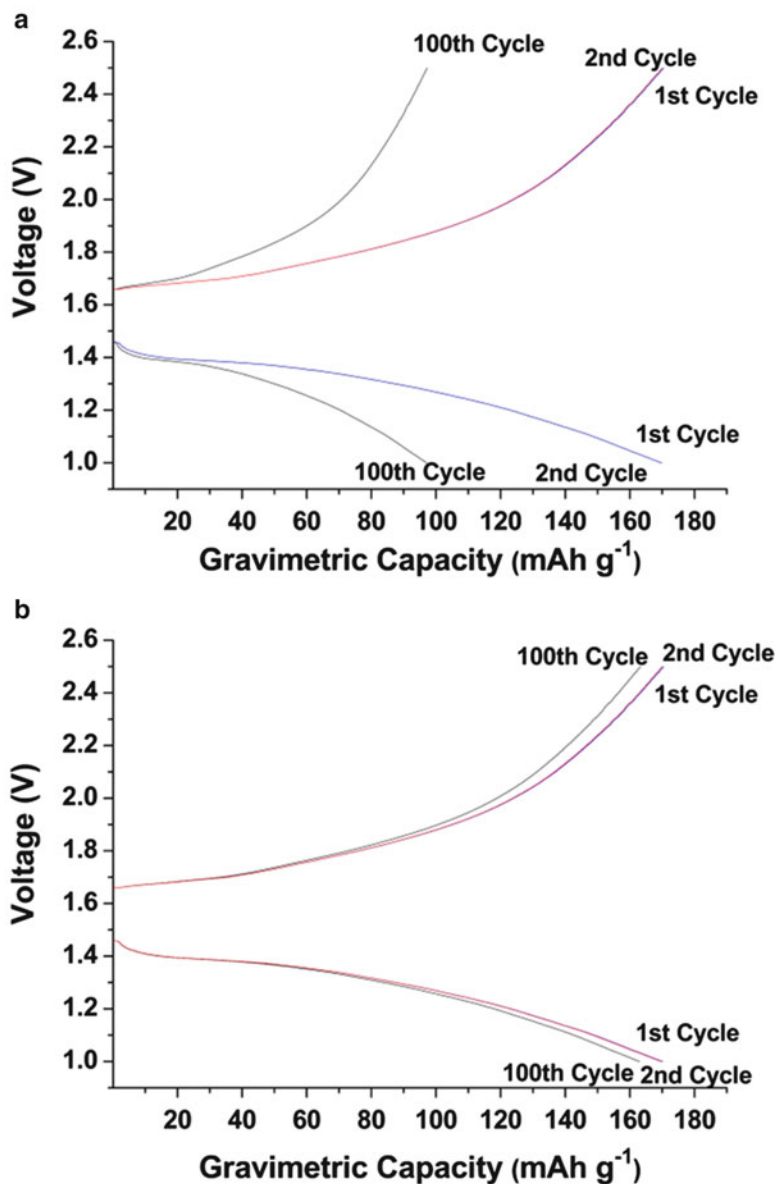


Fig. 2.4 Galvanostatic charge/discharge curves of the (a) pristine LTO and (b) Cu-coated LTO spinel samples

to compare the relationship between the particle size and morphology. The cells were cycled between 1 and 2.5 V at 1 C rate, and an initial capacity of 170 mAh g^{-1} was obtained for both samples which is closer to the theoretical discharge capacity of LTO spinels. Even at 1 C state of charge conditions, the difference between the

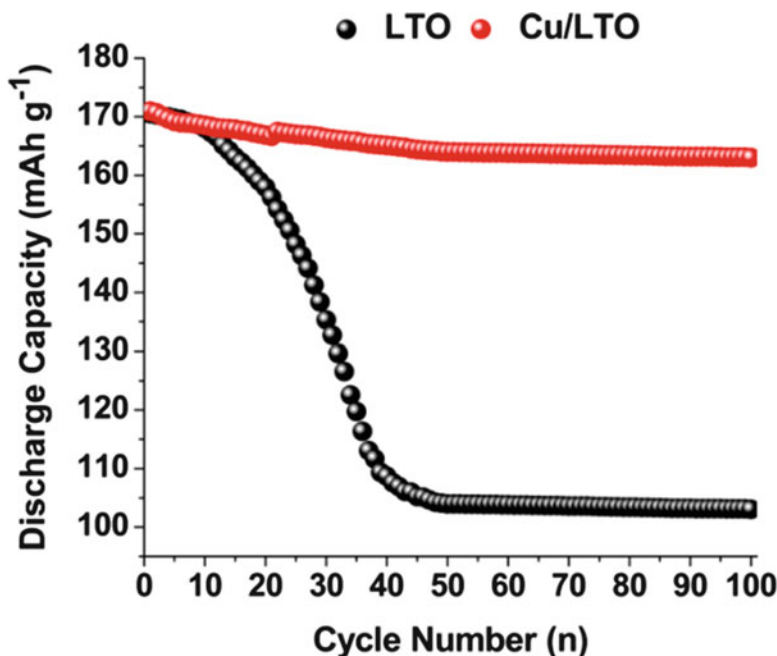


Fig. 2.5 Galvanostatic charge/discharge vs. cycling number curves of the pristine LTO and Cu-coated LTO spinel samples

capacity of the pristine LTO and Cu/LTO is still not so large. This is reasonable because Li^+ insertion/extraction is sufficient at this relatively low current rate. The Li grains in the inner part of the aggregated micron-sized particles are still electrochemically active due to the long diffusion time. However, with increasing the discharge–charge current rate, the difference between the lithium storage capacities of these two samples becomes evident. A specific capacity of 102 mAh g^{-1} and 163 mAh g^{-1} after 100 cycles for pristine LTO and Cu/LTO nanocomposite anode electrodes shows that the Cu coating on LTO samples significantly improved the electronic conductivity of LTO spinels.

Discharge capacity vs. cycle curves of the pristine LTO and Cu/LTO samples were given in Fig. 2.5. It can also be concluded from the figure that the Cu/LTO electrodes show higher lithium storage capability than that made from the pristine powders. Moreover, in addition to the lower capacity, the capacity–cycle profile of the pure sample is not as smooth as that of the Cu/LTO sample, namely, fluctuation of capacity on cycling occurred. Such a capacity fluctuation was also observed by other authors in large aggregated LTO electrode [10, 13]. This capacity fluctuation suggests that the severe aggregation makes the Li^+ insertion/extraction in individual LTO grains inhomogeneous in different cycles. On the contrary, very uniform electrochemical reaction may take place in the well-dispersed LTO nanocomposite electrode, which leads to a very smooth capacity–cycle profile with an average

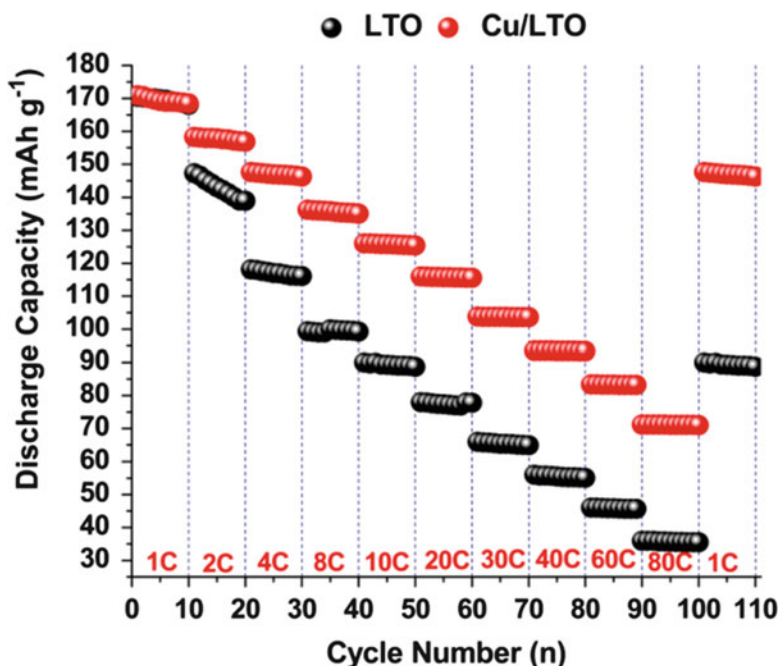


Fig. 2.6 Rate performance of pristine LTO and LTO/Cu composites over the voltage range of 1 and 2.5 V

capacity fading of 2 % per cycle within the first 50 cycles, and no capacity fading has been observed after 50 cycles. The electrochemical data obtained in this study indicates that the cycling performance of the pristine and Cu-coated LTO has been significantly improved. Based on the results from Fig. 2.5, it can be concluded that the Cu-coated LTO had the best cycling performance among pristine LTO.

Figure 2.6 shows the capacity vs. cycle number at various current densities for pristine LTO and Cu/LTO composites. The Cu/LTO samples show much better cycle stability and much better rate capability than pristine samples at the same discharge rate. Upon completion of the 100th charge/discharge cycles, the current density lowers to 1 C again, while the discharge capacity decreases for the first 1 C-rate cycle with a capacity loss of 11 % only for Cu/LTO composites while capacity loss of 47 % for pristine LTO samples. It can also be concluded from Fig. 2.6 that at a low discharge current rate of 1–10 C, the capacity of pristine LTO decays faster and that at a high discharge current rate of 10–80 C, the capacity of Cu/LTO becomes gentle. Figure 2.6 also demonstrates a remarkable rate performance.

Figure 2.7 shows the Nyquist plots of pristine and Cu/LTO composites. The EIS data were collected with a two-electrode coin cell after activation (i.e., after subjecting the coin cell to one charge/discharge cycle). The initial activation was aimed to suppress the Li–electrolyte interfacial resistance that arises from the passivating film formed on lithium metal in contact with the electrolyte. EIS results

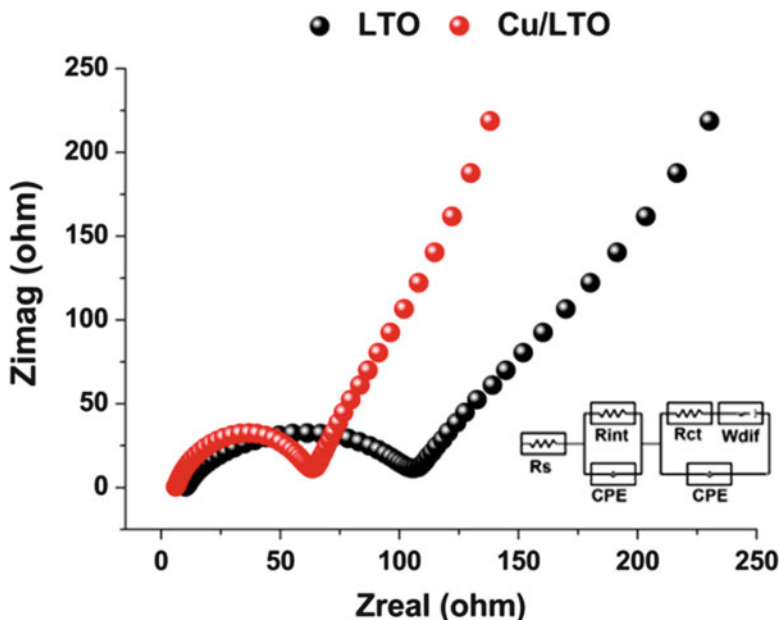


Fig. 2.7 EIS spectra of LTO and Cu/LTO composite electrodes with the frequency range of 10^{-2} – 10^6 Hz

were then fitted with the equivalent circuits inset in Fig. 2.7. On this circuit, R_s is the resistance associated with the electrolyte and cell component, R_{int} is the interface resistance of any film formation of the anode surface (first high-frequency semicircle), R_{ct} is the charge-transfer resistance of the electrode reaction with lithium ions (middle-frequency semicircle), and W_{dif} is the resistance of the lithium ion diffusion to the electrode (low-frequency semicircle). The Nyquist plots of Cu/LTO composites demonstrate unambiguously that the charge transfer of Cu/LTO composite is faster, which can be reflected by the diameter of a semicircle in the medium frequency region. The EIS plots comprised of three parts, and the high-frequency intercept at axis x represents the Ohmic resistance mainly contributed by electrolyte, while the depressed semicircle in the high-to-medium frequency range is normally the charge-transfer resistance and reflects the solid-state diffusion of Li^+ in the bulk of the active material and the constant phase-angle element involving double-layer capacitance. The inclined line in the lower frequency range is attributed to the Warburg impedance, which is associated with the lithium-ion diffusion through the LTO electrode. Apparently, the depressed semicircle of Cu/LTO composites is much smaller than pristine samples calcined, which means that the Cu/LTO composite has better electronic conductivity and ionic conductivities than other samples. Consequently, oxidation of electrolyte and degradation of electrolyte/electrode interface are suppressed effectively by Cu coating, which leads to decreased R_{ct} value and improved electrochemical performance.

2.4 Conclusions

In this study, LTO anode active electrodes were produced via a facile sol–gel process, and Cu/LTO composite electrodes were also prepared using electroless coating process. A pure spinel structure LTO can be obtained by calcination at 850 °C for 1 h. The intimate contact between Cu coating and LTO nanoparticles not only affords a highly conductive matrix for Li-ion insertion but also suppresses the agglomeration and growth of LTO nanoparticles after the calcination process. The confinement of LTO particles in Cu coating reduces lithium-ion and electron transport diffusion resistance. The capacity of Cu/LTO synthesized via electroless coating techniques is 170 mAh g⁻¹ at 1 C rate, and it retains more than 79 and 42 % of its capacity at the discharge rate of 20 and 80 C. Irrespective of the rate used, Cu/LTO basically retain their initial capacity up to 100 cycles at 1 C state of charge conditions. Cu/LTO nanocomposite synthesized at 850 °C is a superior lithium storage material, and it has a promising application in power lithium-ion battery.

Acknowledgments This work is supported by the Scientific and Technological Research Council of Turkey (TUBITAK) under the contract number 111M021—Improving the Capacity of Li-Ion Batteries by Using New Semi-Conducting Metal Oxide Based Anodes. The authors thank the TUBITAK MAG workers for their financial support.

References

1. Yuan T, Wang K, Cai R, Ran R, Shao Z (2009) Cellulose-assisted combustion synthesis of Li₄Ti₅O₁₂ adopting anatase TiO₂ solid as raw material with high electrochemical performance. *J Alloys Compd* 477:665–672
2. Li J, Jin Y-L, Zhang X-G, Yang H (2007) Microwave solid-state synthesis of spinel Li₄Ti₅O₁₂ nanocrystallites as anode material for lithium-ion batteries. *Solid State Ionics* 178:1590–1594
3. Zhu Y-R, Xie Y, Zhu R-S, Shu J, Jiang L-J, Qiao H-B, Yi T-F (2011) Kinetic study on LiFePO₄-positive electrode material of lithium-ion battery. *Ionics* 17:437–441
4. Yi T-F, Jiang L-J, Shu J, Yue C-B, Zhu R-S, Qiao H-B (2010) Recent development and application of Li₄Ti₅O₁₂ as anode material of lithium ion battery. *J Phys Chem Solids* 71:1236–1242
5. Ladislav K, Jan P, Timothy MS, Martin K, Markéta Z, Thierry D, Michael G (2003) Li Insertion into Li₄Ti₅O₁₂ (spinel): charge capability vs. particle size in thin-film electrodes. *J Electrochem Soc* 150:A1000–A1007
6. Borghols WJH, Wagemaker M, Lafont U, Kelder EM, Mulder FM (2009) Size effects in the Li_{4+x}Ti₅O₁₂ spinel. *J Am Chem Soc* 131:17786–17792
7. Naiqing Z, Zhimin L, Tongyong Y, Chenglong L, Zhijun W, Kening S (2011) Facile preparation of nanocrystalline Li₄Ti₅O₁₂ and its high electrochemical performance as anode material for lithium-ion batteries. *Electrochem Commun* 13:654–656
8. Pierre K, Aurélie G, Manfred W, Laurent A, Josette O-F, Jean CJ, Pierre EL (2003) Phase transition in the spinel Li₄Ti₅O₁₂ induced by lithium insertion: influence of the substitutions Ti/V, Ti/Mn, Ti/Fe. *J Power Sources* 119–121:626–631
9. Kiyoshi K, Nao A, Kaoru D (2005) Three dimensionally ordered composite solid materials for all solid-state rechargeable lithium batteries. *J Power Sources* 146:86–89

10. Biao Z, Zhen DH, Sei WO, Jang KK (2011) Improved rate capability of carbon coated $\text{Li}_3.9\text{Sn}_{0.1}\text{Ti}_5\text{O}_{12}$ porous electrodes for Li-ion batteries. *J Power Sources* 196:10692–10697
11. Damien D, Ilias B, Jiwei M, Khalil A (2011) Template-assisted synthesis of high packing density $\text{SrLi}_2\text{Ti}_6\text{O}_{14}$ for use as anode in 2.7-V lithium-ion battery. *J Power Sources* 196:2871–2874
12. Shahua H, Zhaoyin W, Zhonghua G, Xiujian Z (2005) Preparation and cycling performance of Al^{3+} and F^- co-substituted compounds $\text{Li}_4\text{Al}_x\text{Ti}_{5-x}\text{F}_y\text{O}_{12-y}$. *Electrochim Acta* 50:4057–4062
13. Yanling Q, Yudai H, Dianzeng J, Shu JB, Guo ZP (2009) Preparation and characterization of novel spinel $\text{Li}_4\text{Ti}_5\text{O}_{12} - x\text{Br}_x$ anode materials. *Electrochim Acta* 54:4772–4776
14. Shahua H, Zhaoyin W, Xiujian Z, Xuelin Y (2005) Research on $\text{Li}_4\text{Ti}_5\text{O}_{12}/\text{CuxO}$ composite anode materials for lithium-ion batteries. *J Electrochem Soc* 152:A1301–A1305
15. Yan YW, Yan JH, Qiong YL, Ji ZL, Yuan DC, Xiao YJ (2007) A new composite material $\text{Li}_4\text{Ti}_5\text{O}_{12}\text{--SnO}_2$ for lithium-ion batteries. *Ionics* 14:85–88
16. Arumugam S, Sukumaran G, Ramasamy T, Chandrasekaran N, Shanmuga P (2011) Novel $\text{Li}_4\text{Ti}_5\text{O}_{12}/\text{Sn}$ nano-composites as anode material for lithium ion batteries. *Mater Res Bull* 46:492–500
17. Cheng CL, Qiu HL, Li BC, Tai HW (2012) A facile titanium glycolate precursor route to mesoporous $\text{Au}/\text{Li}_4\text{Ti}_5\text{O}_{12}$ spheres for high-rate lithium-ion batteries. *ACS Appl Mater Interfaces* 4:1233–1238
18. Zhimin L, Naiqing Z, Zhijun W, Kening S (2012) Highly dispersed Ag nanoparticles (<10 nm) deposited on nanocrystalline $\text{Li}_4\text{Ti}_5\text{O}_{12}$ demonstrating high-rate charge/discharge capability for lithium-ion battery. *J Power Sources* 205:479–482
19. Yonggang W, Haimei L, Kaixue W, Hosono E, Yarong W, Haoshen Z (2009) Synthesis and electrochemical performance of nano-sized $\text{Li}_4\text{Ti}_5\text{O}_{12}$ with double surface modification of Ti (III) and carbon. *J Mater Chem* 19:6789–6795
20. Hun GJ, Junghoon K, Bruno S, Yang KS (2011) Micron-sized, carbon-coated $\text{Li}_4\text{Ti}_5\text{O}_{12}$ as high power anode material for advanced lithium batteries. *J Power Sources* 196:7763–7766
21. Liang C, Jing Y, Guan NZ, Jia YL, Cong XW, Yong YX (2010) General synthesis of carbon-coated nanostructure $\text{Li}_4\text{Ti}_5\text{O}_{12}$ as a high rate electrode material for Li-ion intercalation. *J Mater Chem* 20:595–602
22. Ilias B, Gary MK, Amine K (2011) Electrochemistry and safety of $\text{Li}_4\text{Ti}_5\text{O}_{12}$ and graphite anodes paired with LiMn_2O_4 for hybrid electric vehicle Li-ion battery applications. *J Power Sources* 196:10344–10350
23. Michal K, Monika M, Bartosz H, Dominika Z, Krzysztof PK, Jacek BJ, Maria K, Ludwika L, Andrzej C (2014) $\text{Li}_4\text{Ti}_5\text{O}_{12}$ modified with Ag nanoparticles as an advanced anode material in lithium-ion batteries. *J Power Sources* 245:746–771
24. Yi RJ, Jenq GD (2012) Synthesis of entanglement structure in nanosized $\text{Li}_4\text{Ti}_5\text{O}_{12}$ /multi-walled carbon nanotubes composite anode material for Li-ion batteries by ball-milling-assisted solid-state reaction. *J Power Sources* 198:294–297
25. Yi RJ, Jenq GD (2012) Electrochemical performance and low discharge cut-off voltage behavior of ruthenium doped $\text{Li}_4\text{Ti}_5\text{O}_{12}$ with improved energy density. *Electrochim Acta* 63:9–15
26. Ting FY, Ying X, Qiuju W, Haiping L, Lijuan J, Mingfu Y, Rongsun Z (2012) High rate cycling performance of lanthanum-modified $\text{Li}_4\text{Ti}_5\text{O}_{12}$ anode materials for lithium-ion batteries. *J Power Sources* 214:220–226
27. Wei F, Xin QC, Peng JZ, Yu LM, Geping Y (2013) A facile strategy to prepare nanocrystalline $\text{Li}_4\text{Ti}_5\text{O}_{12}/\text{C}$ anode material via polyvinyl alcohol as carbon source for high-rate rechargeable Li-ion batteries. *Electrochim Acta* 93:173–178
28. Meng LL, Yu HL, Shih CL, Jing MC, Jien WY, Han CS (2013) $\text{Li}_4\text{Ti}_5\text{O}_{12}$ -coated graphite anode materials for lithium-ion batteries. *Electrochim Acta* 112:529–534
29. Meng LL, Yu HL, Shih CL, Jing MC, Jien WY, Han CS (2013) $\text{Li}_4\text{Ti}_5\text{O}_{12}$ -coated graphite as an anode material for lithium-ion batteries. *Appl Surf Sci* 258:5938–5942
30. Zhenjiang H, Zhixing W, Feixiang W, Huajun G, Xinhai L, Xunhui X (2012) Spherical $\text{Li}_4\text{Ti}_5\text{O}_{12}$ synthesized by spray drying from a different kind of solution. *J Alloys Compd* 540:39–45

31. Feixiang W, Zhixing W, Xinhai L, Huajun G, Peng Y, Xunhui X, Zhenjiang H, Qian Z (2012) Characterization of spherical-shaped $\text{Li}_4\text{Ti}_5\text{O}_{12}$ prepared by spray drying. *Electrochim Acta* 78:331–339
32. Daisuke Y, Yoshihiro K, Jung-Min K, Koichi U, Naoaki K, Naoto K, Yasushi I (2010) Spray-drying synthesized lithium-excess $\text{Li}_{4+x}\text{Ti}_5 - x\text{O}_{12} - \delta$ and its electrochemical property as negative electrode material for Li-ion batteries. *Electrochim Acta* 55:1872–1879
33. Chien-Te H, I-Ling C, Yun-Ru J, Jia-Yi L (2011) Synthesis of spinel lithium titanate anodes incorporated with rutile titania nanocrystallites by spray drying followed by calcination. *Solid State Ionics* 201:60–67
34. Zhaoyin W, Zhonghua G, Shahua H, Jianhua Y, Zuxiang L, Osamu Y (2005) Research on spray-dried lithium titanate as electrode materials for lithium ion batteries. *J Power Sources* 146:670–673
35. Jin YL, Xingcheng X, Drew H, Dongun L, Fathy H, Zhongwei C (2013) Hierarchical $\text{Li}_4\text{Ti}_5\text{O}_{12}$ - TiO_2 composite microsphere consisting of nanocrystals for high power Li-ion batteries. *Electrochim Acta* 108:104–111
36. Milica V, Ivana S, Miodrag M, Slavko M, Nikola C (2013) Hydrothermal synthesis of $\text{Li}_4\text{Ti}_5\text{O}_{12}/\text{C}$ nanostructured composites: morphology and electrochemical performance. *Mater Res Bull* 48:218–223
37. Hui W, Jianfeng J, Hongzhang S, Xing H, Hongwei S, Delin Y (2011) The preparation of Cu-coated Al_2O_3 composite powders by electroless plating. *Ceram Int* 37:2181–2184

Progress in Clean Energy, Volume 2

Novel Systems and Applications

Dincer, I.; Colpan, C.O.; Kizilkan, O.; Ezan, M.A. (Eds.)

2015, XIV, 1184 p. 600 illus., 437 illus. in color.,

Hardcover

ISBN: 978-3-319-17030-5